arXiv:cond-mat/0703126v1 [cond-mat.mtrl-sci] 5 Mar 2007

Anharmonic effects in MgB_2? A comparative inelastic X-ray scattering and Raman study

Matteo d'Astuto[1], Matteo Calandra[1], Stephanie Reich[2], Abhay Shukla[1], Michele Lazzeri[1], Francesco Mauri[1], Janusz Karpinski[3], N.D. Zhigadlo[3], Alexei Bossak[4], and Michael Krisch[4].
[1] *IMPMC, Universités Paris 6 et 7, CNRS, IPGP, 140 rue de Lourmel, 75015 Paris, France.*
[2] *Department of Materials Science and Engineering, Massachusetts Institute of Technology , 77 Massachusetts Avenue, Cambridge, Massachusetts 02139-4307, USA*
[3] *Laboratory for Solid State Physics, ETH Zrich, 8093-Zrich, Switzerland*
[4] *European Synchrotron Radiation Facility, BP 220, F-38043 Grenoble cedex, France*
(Dated: February 6, 2008)

We study anharmonic effects in MgB_2 by comparing Inelastic X-ray and Raman scattering together with *ab-initio* calculations. Using high statistics and high q resolution measurements we show that the E_{2g} mode linewidth is independent of temperature along ΓA. We show, contrary to previous claims, that the Raman-peak energy decreases as a function of increasing temperature, a behaviour inconsistent with all the anharmonic ab-initio calculations of the E_{2g} mode at Γ available in literature. These findings and the excellent agreement between the X-ray measured and *ab initio* calculated phonon spectra suggest that anharmonicity is not the main mechanism determining the temperature behaviour of the Raman-peak energy. The Raman E_{2g} peak position and linewidth can be explained by large dynamical effects in the phonon self-energy. In light of the present findings, the commonly accepted explanation of the reduced isotope effect in terms of anharmonic effects needs to be reconsidered.

PACS numbers: 74.70.Ad, 74.25.Kc, 63.20.Dj, 63.20.Kr, 78.70.Ck, 71.15.Mb

I. INTRODUCTION

The discovery of MgB_2[1] demonstrated that electron-phonon mediated superconductivity can generate critical-temperatures (T_c = 39K) similar to those of perovskite oxides superconducting systems such as cuprates[2] and doped $BaBiO_3$[3]. Almost as surprising as the 39 K critical temperature is the reduced isotope effect[4,5]. The partial isotope coefficients $\alpha(X)$, defined as $\alpha(X) = -\frac{d\ln T_c}{d\ln M_X}$ where M_X is the atomic mass of ion X, are $\alpha(B) = 0.30(1)$ and $\alpha(\mathrm{Mg}) = 0.02(1)$. Thus, the total isotope coefficient of $\alpha \approx 0.32$ is substantially reduced from the canonical BCS value of $\alpha_{BCS} = 0.5$.

Deviations from α_{BCS} value are usually attributed to strong electron-phonon coupling and to Coulomb repulsion. However, theoretical investigations of the isotope coefficient using single- or double-gap Migdal-Eliashberg equations[6,7] lead to unsatisfactory results since the isotope effect reduction is substantially underestimated. For this reason, it was proposed[6,7,8,9] that the T_c in MgB_2 is determined by the interplay of electron-phonon coupling and anharmonic effects. The latter can reduce T_c through a hardening of the phonon frequencies. Refs.[6,7] showed than a hardening of ≈ 25% of the E_{2g} phonon-frequency, along the high symmetry direction ΓA, would be necessary to explain the reduced isotope-coefficient.

Anharmonic effects contribute to the broadening of a phonon and determine energy shift from its harmonic value. The anharmonic shift can be determined from the actual experimental phonon energy and from the harmonic energy, obtained from *e.g.* calculations. The intrinsic linewidth of a phonon is, in general, given by two contributions due to anharmonicity and electron-phonon coupling. The anharmonic linewidth can, thus, be determined from the actual experimental linewidth and from the electron-phonon linewidth obtained *e.g.* by calculations. Finally, the temperature dependence of the phonon energy and linewidth is usually almost entirely due to the anharmonicity. The experimental determination of the temperature dependence of the phonon energy and linewidth thus provide a further source of information.

Raman spectra of MgB_2[10,11,12,13,14,15,16,17] show a single very-broad peak corresponding to an excitation with E_{2g} symmetry at 75 meV, (*i.e.* 15% higher than the theoretical harmonic frequency of 65 meV). Furthermore, the linewidth of the peak has a very strong temperature dependence. These two facts have been interpreted by several authors[6,8,9,12,18,19] as a signature of strong anharmonicity. The presence of strong anharmonic-effects was further supported by ab-initio calculations based on the frozen-phonon model[6,8,9,12,15,18,19]. However, the results obtained with this model are questionable, since the frozen-phonon approximation is an oversimplified model which does not include all the terms of the anharmonic perturbation theory[20,21,22,23,24].

Ab-initio calculations of anharmonic effects including all the leading terms in anharmonic perturbation theory (including scattering between different wavevectors and different phonon modes)[23,25] show that the phonon frequency shift of the E_{2g} mode is only 5% of its harmonic phonon frequency at Γ. This is the result of a partial cancellation between a large positive four-phonon scattering term (≈ +10%) and a negative three-phonon scattering term (≈ −5%). This is different from what is found by the more-approximate frozen-

phonon calculations, where the four-phonon scattering term is dominant[6,8,9,12,15,18,19]. This difference should be reflected in the temperature dependence of the Raman-peak energy, since the four-phonon scattering term generates an increase in energy with temperature, while the sum of three- and four-phonons term should be slightly negative[23,24].

Inelastic X-ray scattering (IXS) measurements do not support the hypothesis of strong anharmonic effects. In fact, the phonon dispersion measured by IXS[25,26] is in good agreement with harmonic-frequency calculations[25,27] and is consistent with a small anharmonic shift along the ΓA direction. In particular, the IXS E_{2g} phonon frequency near Γ is 65 meV, *i.e.* ∼10 meV smaller than the Raman peak. Ab-initio calculations of the phonon linewidth are in very good agreement with IXS measurements[25] and give an anharmonic contribution to the phonon linewidth which is negligible with respect to the larger electron-phonon coupling contribution. Moreover, calculations[25] reveal a very weak temperature-dependence of the phonon-linewidth between 50 K and 300 K. Finally, the authors of Ref.[26] claim that the phonon-linewidth of the E_{2g} mode is independent from temperature between 40 K and 300 K along the ΓA. If confirmed, this last finding would establish that anharmonic effects are weak. However, the moderate resolution and the fact that in Ref.[26] the E_{2g} mode is seen only as a shoulder of the nearby E_{1u} mode do not allow for a definitive conclusion.

In this work we present a high-resolution inelastic X-ray scattering and Raman study, in order to settle the debate on the presence of important anharmonic effects in MgB_2. The two techniques are complementary since inelastic X-ray scattering probes the phonon dispersion throughout the entire Brillouin zone. However, at the Γ point the elastic (Bragg) scattering usually dominates, therefore masking the phonon contributions, as it is the case in MgB_2. On the contrary, Raman experiments probe excitations at very small exchanged momentum, $\mathbf{q} \sim 0$. We show with high statistics and high q-resolution IXS measurements that the E_{2g} mode linewidth is independent of temperature along Γ-A, and furthermore determine the dispersion along Γ-M with the best resolution to date. We investigate the behaviour of the Raman-peak energy and linewidth as a function of temperature. All our results are consistent with the presence of small anharmonic effects in MgB_2. We, finally, show that, on the basis of recent theoretical results[24,28,29], there is no contradiction between the presence of a Raman-peak at 75 meV and the X-ray E_{2g} phonon frequency at 65 meV *near* Γ.

The paper is structured as follows. In sec. II we describe the methodological details involved in inelastic X-ray scattering, Raman spectroscopy and *ab-initio* simulations. In sec. III we present our main results and in sec. IV we comment on the results and discuss the main implications for the interpretation of Raman data.

II. METHODS

A. Experiments

1. Sample

The crystal used in our experiment was grown at a pressure of 30-35 kbar. A mixture of Mg and B was put into a BN container in a cubic anvil device. The temperature was increased during one hour up to $1700-1800°C$, kept stable for 1-3 hours, and finally decreased during 1-2 hours. As a result plate-like MgB_2 crystals were formed of which we used a sample of about $1.00\times0.45\times0.08$ mm^3 with a measured in-plane mosaic of 0.011°.

2. Inelastic X-ray Scattering

The experiment was carried out at the Inelastic X-ray Scattering Beamline II (ID28) at the European Synchrotron Radiation Facility in Grenoble (France). The x-ray beam from the undulators was monochromatized by a cryogenically cooled silicon (111) double crystal monochromator, followed by a back-scattering monochromator, operating at a Bragg angle of 89.98 degrees, and utilizing the Si (9 9 9) reflection order[30]. The back-scattered beam was then focused by a platinum-coated toroidal mirror, which provided a focal spot at the sample position of 0.270 (horizontal) and 0.080 mm^2 FWHM at the sample position. The scattered photons were energy-analyzed by a 6.5m Rowland circle five-crystal-spectrometer[31,32]. The analysers operate at the same reflection order as the monochromator, corresponding to a wavelength $\lambda = 0.696782$ Å^{-1} (photon energy: 17794 eV). The overall instrumental function has a pseudo-Voigt line-shape with a width ΔE of 3 meV (FWHM) as determined from the elastic scattering of a Plexiglas sample (at a Q-transfer of 10 nm^{-1}, and T = 10 K). The energy-analyzed photons are detected by a Peltier-cooled silicon diode detector which has an intrinsic energy resolution of 400 eV. The dark counts due to electronic and environmental noise amounts to about 0.2 counts/minute. Further components of the spectrometer are an entrance pinhole, slits in front of the analysers in order to define the momentum transfer resolution and a detector pinhole for aberrant ray suppression.

The analyser crystals are temperature stabilized at 295.65 K with a typical stability of 1 mK/24h. The momentum transfer $Q = 2\ k_i\ \sin(\frac{\theta}{2})$, where k_i is the incident photon wave vector and θ, the scattering angle, is selected by rotating the spectrometer around a vertical axis passing through the scattering sample in the horizontal plane. Since there are five independent analyser systems, spectra at five different momentum transfers can be recorded simultaneously. Their separation is energy dependent and for the Si(9 9 9) reflection it amounts to 2.43 nm^{-1}. The energy scans are performed by varying

the lattice spacing of the monochromator temperature while the analyser temperature is kept fixed. Conversion from the temperature scale to the energy scale is accomplished by using the known thermal expansion coefficient of silicon: $\alpha(\mathrm{T}) = \alpha_0 + \beta\ (\mathrm{T}\text{-}\mathrm{T}_0)$ with $\alpha_0 = 2.581 \times 10^{-6}$ 1/K and $\beta = 0.016 \times 10^{-6}$ 1/K^2, $\mathrm{T}_0 = 295.65$ K[33].

The validity of this conversion has been checked by comparing the measured diamond dispersion curve for longitudinal acoustic and optic phonons with well established inelastic neutron scattering results.

The energy scans were fitted using a sum of pseudo-Voigt:

$$I\left((1-\eta)\frac{\Gamma/2}{(\epsilon-\epsilon_0)^2+\Gamma^2/4}+\eta\exp\left(-\frac{(\ln 2)(\epsilon-\epsilon_0)^2}{\Gamma^2/4}\right)\right) \tag{1}$$

and Lorentzian functions:

$$I\frac{\Gamma/2}{(\epsilon-\epsilon_0)^2+\Gamma^2/4} \tag{2}$$

functions, where $\epsilon = \hbar\omega = h\nu$ is the energy. Pseudo-Voigt functions were used to fit elastic and resolution-limited inelastic contributions, with Γ and η parameters adapted to match the instrumental function, while a Lorentzian line-shape was used to fit the E_{2g} mode, with a width Γ fitted to the data. Alternatively, a convolution with the experimental resolution function has been used. In this case, the response function was composed of a sum of delta functions (for elastic and resolution-limited inelastic contributions) plus a Lorentzian for the E_{2g} mode. The two data analysis procedures gave consistent results.

The fitting algorithm used a χ^2-minimisation routine[34], with the condition that the detailed balance between Stokes and anti-Stokes excitations is fulfilled. A constant background, coming essentially from electronic noise, was added.

The MgB_2 crystal was glued on a copper sample holder, which was mounted inside a vacuum chamber on the cold finger of a closed-loop helium cryostat (Cryomech ST15). The temperature was measured by a silicon diode attached to the sample holder. An independent check of the sample temperature was provided by the Stokes-Anti-stokes intensity ratio.

3. Raman measurements

Raman spectra were excited with the 488 nm line of an Ar laser focused with an optical microscope (long distance 100x objective). The scattered light was analyzed by a single-grating LABRAM spectrometer equipped with a CCD. Temperature dependent measurements were performed in an OXFORD flow cryostat with a sapphire window to preserve the polarization of the light. We used a 600 1/nm grating to record a wide spectral window (5000 cm^{-1} or 620 meV). The loss in resolution is irrelevant for MgB_2, because its Raman features are at least several hundreds of wave numbers in width. Some experiments were also performed with 514 nm and a triple-grating spectrometer to compare with published studies. We report the as-measured data normalized to the excitation energy and accumulation time. Unless noted otherwise, the spectra were not scaled or shifted along the y axis.

To analyze the symmetry of the scattered light we recorded Raman spectra in various backscattering geometries $k_i(e_i, e_s)k_s$, where k_i and k_s indicate the direction of the incoming (i) and scattered (s) light and e_i and e_s the polarization (Porto's notation)[35]. For $\boldsymbol{k_i}\|\boldsymbol{k_s}\|c$ we used backscattering normal to the surface; in the $\boldsymbol{k_i}\|\boldsymbol{k_s}\|a, b$ configurations the laser was focused onto the side of a MgB_2 crystal. The polarization of the incoming light was rotated by a Fresnel rhomb. The polarization of the scattered light was chosen by a $\lambda/2$ wave plate combined with an analyzer. We verified the polarization-dependent measurements by recording spectra on the (111) and (001) surface of silicon and on single crystals of graphite, which has the same point group as MgB_2. We also ensured the internal consistency of the Raman intensities; e.g., the spectra recorded in $c(a, a)c$ and $b(a, a)b$ were identical in shape and intensity as required by the Raman selection rules.

The frequency of the $\sim 600\,\mathrm{cm}^{-1}$ (74 meV) peak of MgB_2 reported in the literature varies between 74 and 77 meV at room temperature.[10,13,14,16,36] Part of the discrepancy might be due to a varying sample quality. However, a major contribution comes from the uncertainty resulting from the functional form used for the background and the peak. We tested several fitting routines and found that the uncertainty for the position and width of a Lorentzian is around 1.5% or 1.2 meV. On the other hand, when using a Fano line-shape the bare phonon frequency can be as low as 71 meV or as high as 79 meV (300 K) depending on the sign of the asymmetry parameter. The peak positions and line widths reported in this paper were obtained by assuming the 600 cm^{-1} peak to be Lorentzian and the continuous background in the E_{2g} spectra to follow the same frequency dependence as the $\alpha_{xx}(A_{1g})$ background signal (see Sect. III B 1 for details). Other fit functions shift the position and width. We also observed a change in the phonon frequency when reducing the energy range in a fit. For our analysis we used the measured spectra between 100 and 2000 cm^{-1} ($\sim$ 10 and 250 meV). Smaller windows yield a strong scattering in the peak positions. We stress, however, that varying fit routines resulted in a constant offset of the temperature dependence or stronger scattering in the data. The functional dependence of the Raman peak position and width on temperature, however, remained unaffected.

B. Calculations

Electronic structure calculations were performed using density functional theory (DFT) and phonon frequencies were calculated in the framework of linear response theory[37] using the PWSCF/espresso package[38]. We used the generalized gradient approximation[39] and norm conserving pseudo-potentials[40]. For Mg we used non-linear core corrections[41] and we treated the $2s$ and $2p$ levels as core states. The wave-functions were expanded in plane waves using a 35 Ry cutoff. The calculations were performed with the experimental crystal structure, namely $a = 3.083$ Å and $c/a = 1.142$. For the phonon frequencies calculation, we used a $16 \times 16 \times 16$ Monkhorst-Pack grid for the electronic Brillouin Zone integration and first order Hermite-Gaussian smearing[42] of 0.025 Ry.

The electron-phonon coupling contribution to the linewidth (full width half maximum) at momentum $\mathbf{q}$ for the ν phonon mode, with frequency $\omega_{\mathbf{q}\nu}$ can be written as[43]:

$$\gamma_{\mathbf{q}\nu} = \frac{4\pi\omega_{\mathbf{q}}}{N_k} \sum_{\mathbf{k},n,m} |g^{\nu}_{\mathbf{k}n,\mathbf{k}+qm}|^2 \delta(\varepsilon_{\mathbf{k}n})\delta(\varepsilon_{\mathbf{k}+qm}) \quad (3)$$

where the $\mathbf{k}$-sum is extended over the Brillouin Zone , N_k is the number of k-points in the sum, and $\varepsilon_{\mathbf{k}n}$ are the electronic energies, measured with respect to the Fermi level, of the n band at point $\mathbf{k}$. The matrix element is $g^{\nu}_{\mathbf{k}n,\mathbf{k}+\mathbf{q}m} = \langle \mathbf{k}n|\delta V/\delta e_{\mathbf{q}\nu}|\mathbf{k}+\mathbf{q}m\rangle/\sqrt{2\omega_{\mathbf{q}\nu}}$, where $\delta V/\delta e_{\mathbf{q}\nu}$ is the derivative of the Kohn-Sham potential V with respect to the phonon coordinate $e_{\mathbf{q}\nu}$ normalized over the unit cell.

The electron energies $\varepsilon_{\mathbf{k}n}$ and the $g^{\nu}_{\mathbf{k}n,\mathbf{k}+\mathbf{q}m}$ matrix element in eq. 3 are obtained fully *ab initio*. The actual sum over the Brillouin zone is calculated on a $N_k = 27\times27\times27$ uniform k-point mesh shifted by a random vector with respect to the origin.

The x-ray structure factor for one-phonon scattering at temperature T, frequency ω and reciprocal-space vector $\mathbf{q} + \mathbf{G} = \mathbf{Q}$ (with $\mathbf{q}$ belonging to the first Brillouin Zone and $\mathbf{G}$ a reciprocal-lattice vector, and $\mathbf{Q}$ the total momentum transfer) is obtained from

$$S(\mathbf{Q},\omega) = \sum_{\nu} G_{\nu}(\mathbf{q},\mathbf{G}) F_{\nu}(\omega,T,\mathbf{G}) \quad (4)$$

with

$$G_{\nu}(\mathbf{q},\mathbf{G}) = \left| \sum_{\alpha} f_{\alpha}(\mathbf{Q}) \frac{e^{-W_{\alpha}}}{\sqrt{M_{\alpha}}} \left[(\mathbf{Q})\cdot\mathbf{e}^{\alpha}_{\mathbf{q}\nu}\right] e^{i\mathbf{Q}\mathbf{R}_{\alpha}} \right|^2$$

$$F_{\nu}(\omega,T,\mathbf{G}) = \sum_{\eta=-1}^{1} \frac{\langle n_{\mathbf{q}\nu}\rangle + \frac{1}{2} + \frac{\eta}{2}}{\omega_{\mathbf{q}\nu}} \cdot \delta(\omega + \eta\omega_{\mathbf{q}\nu}) \quad (5)$$

where α labels the atoms in the unit cell, ν the mode and $f_{\alpha}(\mathbf{Q})$ is the atomic form factor calculated as in [44]. Moreover, M_{α}, $\mathbf{R}_{\alpha}$ and W_{α} are the atomic mass, position in the unit cell and the Debye-Waller factor, respectively. Finally, $\langle n_{\mathbf{q}\nu}\rangle$ is the phonon occupation number and $\mathbf{e}^{\alpha}_{\mathbf{q}\nu}/\sqrt{M_{\alpha}}$ is the atomic displacement of the atom α corresponding to the phonon eigenvector $\mathbf{e}_{\mathbf{q}\nu}$. The value $\eta = -1$ ($\eta = 1$) identifies Stokes (anti-Stokes) processes.

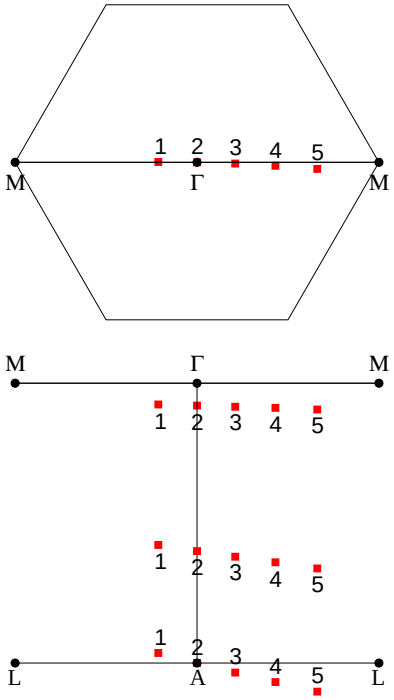

FIG. 1: (Color online) Positions of the analyzers (red squares) for the measurements along Γ-A (see Fig. 6), and near Γ (see Fig. 5). Γ=G(HKL)=(2,1,0).

In what follows we neglect the Debye-Waller factor and we smear the $\delta-$functions with the convolution between the phonon intrinsic lineshape calculated *ab initio* and the instrumental function (3 meV FWHM). For the calculation of the x-ray structure factor we used the atomic factors for neutral Mg and B from[44] and the phonon patterns calculated *ab initio*.

III. RESULTS

A. Inelastic X-ray Scattering results

The reciprocal points in the following section are expressed in terms of hexagonal parameters $a = b = 3.0828$, Å $c = 3.5186$ Å, $\alpha = \beta = 90°$ and $\gamma = 120°$. In these coordinates, all the measurements were recorded in the Brillouin Zone centered around (2,1,0).

In Fig. 1 and 2 we show the relative position of the analyzers for the measurements reported below.

1. *Dispersion along* Γ-*M*

The experimental results shown in figure 3 were obtained exploiting the signal from all five analyzers. The

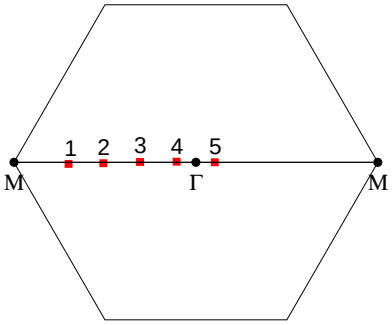

FIG. 2: (Color online) Positions of the analyzers (red squares) for measurements along Γ-M (see Fig. 4). Γ=G(HKL)=((2,1,0).

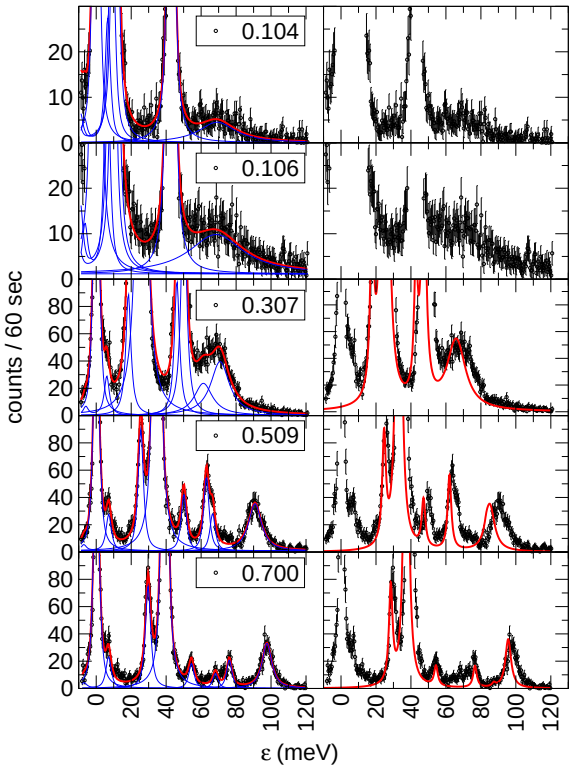

FIG. 3: (Color online) Left: IXS data (circle) and fit (lines) along Γ-M for T=46 K. Right: IXS data (circle) and calculations (lines) along Γ-M for T=46 K. The legend box indicate the ξ components of the **q** reduced vector (see text).

relative Q displacement between the analyzers is fixed by the spectrometer geometry, and for longitudinal modes such a configuration can be close to a high symmetry direction. This opportunity has been as well exploited in previous works on MgB_2[25,26]. Here the difference is that, using a different incoming wavelength of 0.696782 $Å^{-1}$, we have higher energy resolution and larger steps in reciprocal space, corresponding to the different fixed angular displacement of the analyzers. For a position

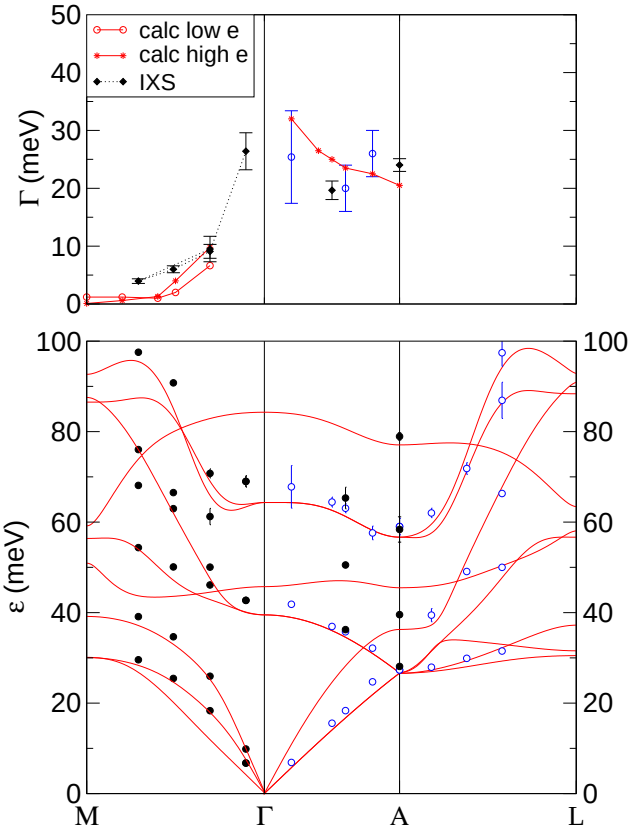

FIG. 4: (Color online) Bottom panel: MgB_2 phonon dispersion. IXS data (circles) from[25] (blue open) and the present work (black full), compared to calculations (red lines). Top panel: E_{2g} mode width from fit of the IXS data of the present work (black diamonds) and Ref.[25] (blue open with errorbars) and calculations (red points with continuous line connected). Stars corresponds to the high energy and open circles to the low energy E_{2g} modes when not degenerate.

close to the Γ-M line, this implies Q points G + q = $(2,1,0)+(\xi,\upsilon,\zeta)$ where υ and ζ are small compared to ξ. The configuration chosen for this experiment was as follows:

- analyzer 5: Q = (2.052 1.000 0.0), $|\xi| \approx 0.052$ or 0.104 Γ-M;
- analyzer 4: Q = (1.948 1.002 0.0), $|\xi| \approx 0.053$ or 0.106 Γ-M ;
- analyzer 3: Q = (1.847 1.001 0.0), $|\xi| \approx 0.1535$ or 0.307 Γ-M;
- analyzer 2: Q = (1.744 0.997 0.0), $|\xi| \approx 0.2545$ or .509 Γ-M;
- analyzer 1: Q = (1.645 0.990 0.0), $|\xi| \approx 0.350$ or 0.700 Γ-M;

The positions in the hexagonal plane are shown in Fig. 2. Note that analyzers 4 and 5 are placed symmetrically around the chosen zone center. These positions are

equivalent for phonon frequencies but not for dynamical structure factors. Contribution along $< 0, \upsilon, 0 >$ are less than 0.005 r.l.u. for analyzer 5 to 2 and 0.01 r.l.u. for analyzer 1.

We measured the IXS spectra using a slit opening in front of the analyzers of 60 mm in both horizontal and vertical direction, amounting to a Q resolution of ± 0.416 nm^{-1} for analyzers 1, 2 and 3, while analyzers 4 and 5 had 60 × 20 mm^2 vertical × horizontal opening. This corresponds to a main contribution of ± 0.0022 r.l.u. in the (0 , υ , 0) direction and to ± 0.008 r.l.u. in the perpendicular (0 , 0 , ζ) (or Γ-A) direction.

In Fig. 3, left panel, we show the IXS spectra obtained at ≈ 46 K for this configuration, together with the fit used in order to extract mode frequencies as well as linewidth values for the E_{2g} mode. A recent paper[45] suggests that the MgB_2 IXS spectra show additional structures due to two-phonon contributions. Although we do not have analyzed our data in this way, such contributions may actually explain small deviations of our fit results. In the right panel we show the same data compared with *ab-initio* calculated spectra, which correctly reproduce the measurements.

The same analysis is done for points along Γ-A (see Sec. III A 3). These are grouped together with previous results at lower resolution[25] in order to experimentally determine the phonon dispersion and the linewidths along all the high symmetry directions. We can thus compare the experimental phonon dispersion with the theoretical calculation along the high symmetry lines, as shown in Fig. 4, bottom. In the top panel, we show the experimental line-width Γ, for the E_{2g} mode, de-convoluted by the instrumental broadening, in comparison with the calculated linewidth. The agreement of the calculated frequencies with experiment is remarkable. The same is observed for the agreement between the experimental linewidth, de-convoluted by the instrumental function, and the calculated electron-phonon-coupling contribution to the intrinsic E_{2g} linewidth. Note that data from Ref.[25] are obtained at room temperature and with 6.1 meV instrumental function FWHM.

2. *High resolution line-width E_{2g} measurements close to* Γ

Fig. 5 shows the room temperature MgB_2 IXS spectra for a Q-value corresponding to 0.08×Γ-A, together with the data, we show calculation convoluted with the instrumental resolution for all modes, including the E_{2g} one. The calculation was scaled as in Fig. 6.

We measured the IXS spectra using a slit opening in front of the analyzers of 20 mm in both horizontal and vertical direction, equivalent to a Q resolution of ± 0.139 nm^{-1}. This corresponds to a main contribution of ± 0.0022 reduced lattice units (r.l.u.) in the (0 , υ , 0) direction and to ± 0.0026 r.l.u. in the perpendicular (0 , 0 , ζ) (or Γ-M) direction.

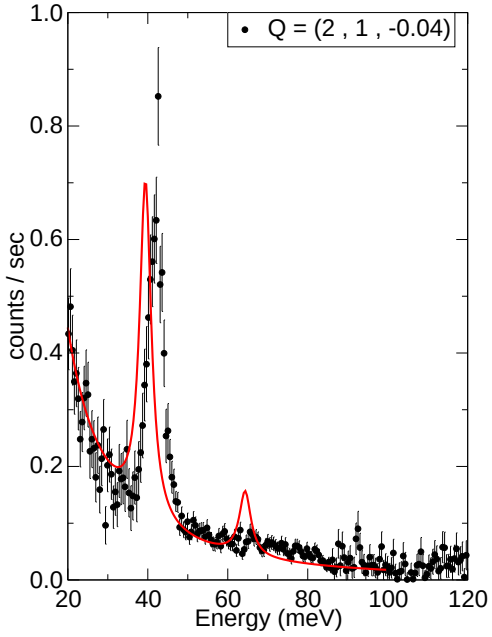

FIG. 5: (Color online) Room temperature IXS data at 0.08×Γ-A. The line is an ab-initio simulation convoluted with the energy resolution, ***without electron-phonon coupling*** broadening effect on the E_{2g} mode.

3. *Temperature-dependence of the IXS spectra*

In figure 6 we compare IXS E_{2g} spectra measurements and calculations performed at two different sample temperatures ($\sim$ 50 K and 300 K) for Q=(HKL) corresponding to a phonon propagation vector of (0, 0, 0.3) (top panel) (*i.e.* at 60% of the Γ-A line) and the zone boundary A point (0 , 0 , 0.5) (bottom panel).

To induce a maximum effect from phonon-phonon scattering (anharmonicity)[23,25], we choose the largest possible temperature difference in the normal-state region, *i.e.* from room temperature to T above $\sim$ 40 K. This was done to avoid effects due to the superconducting gap. More precisely, the measured temperature by the probe on the sample holder was stable at 46 K and 298 K respectively.

We measured the IXS spectra using a slit opening in front of the analyzers of 60 mm in both horizontal and vertical direction, equivalent to a Q resolution of ± 0.416 nm^{-1}. This corresponds to a main contribution of ± 0.0065 r.l.u. along the (0 , υ , 0) direction and to ± 0.008 r.l.u. along the perpendicular (0 , 0 , ζ) direction (*i.e.* along Γ-A). The theoretical spectra are arbitrarily normalized to reproduce the height of the highest vibrational peak (E_{1u}, not shown in Fig. 6.)

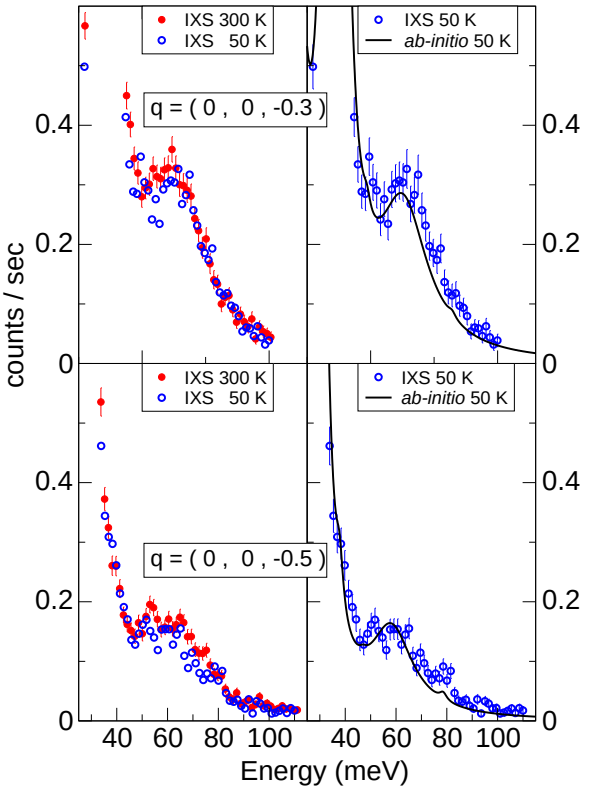

FIG. 6: (Color online) Left: IXS data at T=300 K (red full points, with errorbars) and T=46 K (blue empty points). Right: IXS data at T=46 K (blue empty points) and ab-initio simulation (lines) Measured spectra and calculation spectra at 0.6×Γ-A (top) and at the A point (bottom).

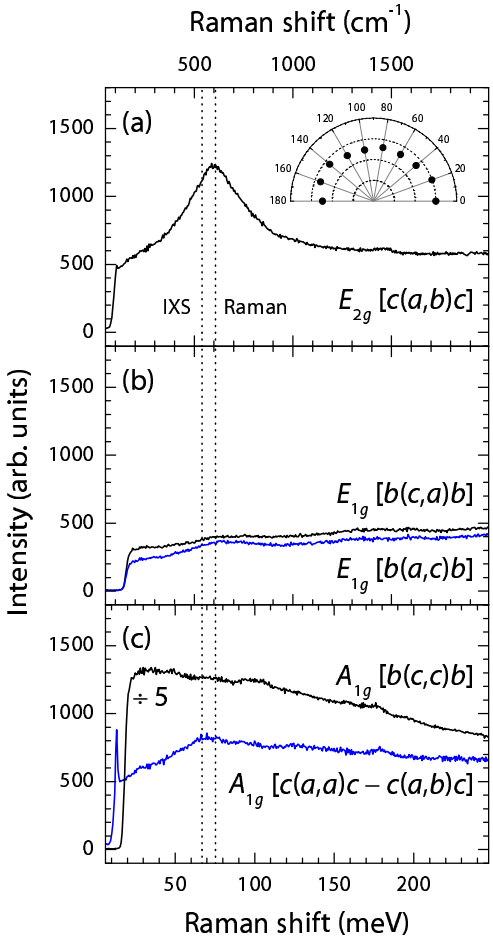

FIG. 7: (Color online) Raman selection rules and symmetry of the scattered light in MgB_2 (room temperature). (a) E_{2g} component with the peak at 75 meV (608 cm^{-1}). The background measured under crossed polarization is also of E_{2g} symmetry in contrast to parallel polarization, where it has E_{2g} and A_{1g} [see (c)] contribution. The inset shows the constant integrated intensity of the 75 meV peak when rotating the in-plane polarization. (b) E_{1g} symmetry obtained in two scattering configurations. (c) α_{zz} and $\alpha_{xx} = \alpha_{yy}$ A_{1g} component of the scattering intensity. The latter was obtained by subtracting the $c(a,a)c$ and $c(a,b)c$ Raman spectra. The two dashed lines mark the phonon frequency of the E_{2g} peak measured with Raman and inelastic X-ray scattering.

TABLE I: Raman selection rules for the D_{6h} point group of MgB_2. a and b are vectors within the hexagonal plane forming an angle of 90°. Since the hexagonal lattice is isotropic in the plane a and b can be chosen arbitrarily (with respect to the lattice vectors). c is normal to the plane. The α_{ii} denote the element ii of the corresponding Raman tensor.

configuration	Raman intensity	symmetry
$c(a,a)c$, $b(a,a)b$	$\alpha_{xx}^2 + \alpha_{yy}^2$	A_{1g}, E_{2g}
$c(a,b)c$, $c(b,a)c$	α_{xy}^2	E_{2g}
$b(c,c)b$	α_{zz}^2	A_{1g}
$b(a,c)b$, $b(c,a)b$	α_{xz}^2	E_{1g}

B. Raman results

1. *Raman selection rules*

Table I gives the selection rules for the Raman active representations of MgB_2 (D_{6h} point group). Note that the intensity of E_{2g} is independent of polarization as long as the light incidents and scatters normal to the ab plane. In Fig. 7 we present the four independent components of the Raman scattered light from the MgB_2 crystal. The ∼ 75 meV peak is indeed only found in the E_{2g} scattering configuration,[10,13] Fig. 7(a), and its intensity is independent of the in-plane orientation of the crystal (see inset). The weak feature at 75 meV in the E_{1g} $b(a,c)b$ configuration is within experimental error. The two dotted lines mark the E_{2g} peak frequency as obtained by Raman (75 meV) and inelastic X-ray scattering (≈ 69 meV) at 0.1 Γ-M and *ab-initio* calculations at Γ (70 meV)[23]. As noted earlier, the two measurements give phonon frequencies differing by at least ∼ 6 meV.

Our Raman spectra, consistently with the literature[10,11,12,13,14,15,16,17], are smooth. They do not show any structure that can be interpreted as a multiple-phonon peak, as proposed in Ref. 45. In

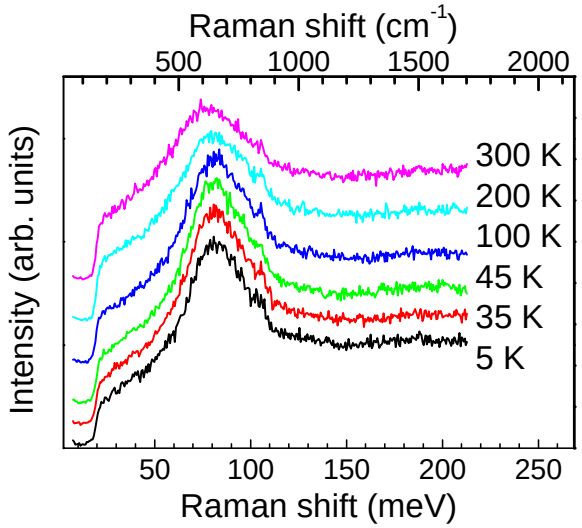

FIG. 8: (Color online) E_{2g} Raman spectra (raw data) of MgB_2 between 5 K and room temperature in $c(a,b)c$ scattering configuration. An offset has been added for clarity (see the zero line at the cut-off of the notch filter).

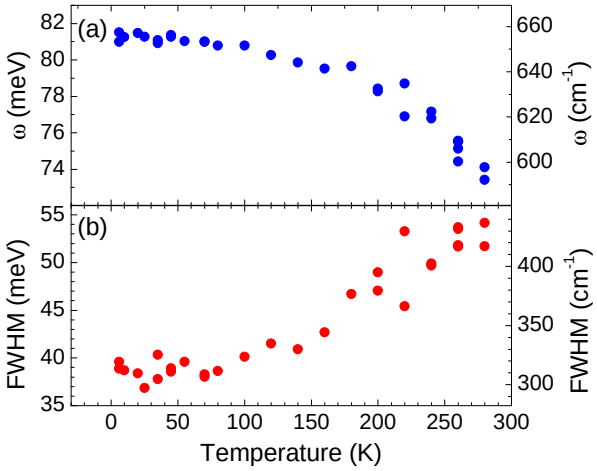

FIG. 9: (Color online) Position (a) and full width at half maximum (b) for the 75 meV (600 cm^{-1}) Raman peak. The spectra were fitted by a Lorentzian plus a background. The frequency dependence of the background is assumed to be the same as the $\alpha_{xx}(A_{1g})$ component, see Fig. 7(c).

general, two-phonon Raman spectra have more than one symmetry component[35]. However the A_{1g} and E_{1g} spectral contributions in Fig. 7 do not show any sharp feature.

The polarization dependence of the continuous background for $\alpha_{xz}(E_{1g})$, Fig. 7(b), and $\alpha_{zz}(A_{1g})$, Fig. 7(c), agree with Quilty *et al.*[10]. The scattering intensity increases linearly with the frequency of the excitation. We extracted the $\alpha_{xx}(A_{1g})$ background component from the measured spectra as shown in Fig. 7(c). In contrast to the frequency dependence of the zz and xz component of the Raman tensor, α_{xx} has a maximum at ~ 60 meV and decreases in intensity towards smaller frequencies. The $\alpha_{xy}(E_{2g})$ background component appears to be similar to $\alpha_{xx}(A_{1g})$; the overall intensity is almost identical and the decrease in background intensity towards small frequencies is present as well as can be seen in Fig. 7(a). This points towards a common origin of the electronic E_{2g} and A_{1g} scattering, e.g., such a behavior might arise from a coupling of electrons that are correlated with the E_{1g} representation of the MgB_2 point group.

The precise origin of the electronic background in the MgB_2 Raman spectra is not known. It is remarkable that the signal is strong and approximately constant over a wide energy range (at least up to 600 meV the highest energy in our measurements).

2. *Temperature-dependence of the Raman spectra*

Figure 8 shows Raman spectra measured between 5 K (bottom) and room temperature (top). The 75 meV (600 cm^{-1}) peak decreases in frequency and broadens at higher temperatures. The frequency shift is more pronounced than reported by Quilty *et al.*[10] and disagrees with the finding by Martinho *et al.*[14], who reported a constant peak frequency between 10 and 300 K. The shift in the peak maximum agrees with Rafailov *et al.*[16], although this is somewhat difficult to judge given the narrow Raman frequency window in the reference. Surprisingly, we find the electronic background to be independent of temperature. The intensity is constant (the spectra in Fig. 8 are raw data) and there is no increase in the scattering intensity at low frequency for low T[10,36].

The frequency of the $\sim$ 75 meV (600 cm^{-1}) Raman peak decreases from 81 meV to 75 meV between 5 K and room temperature as we show in Fig. 9(a). This is accompanied by an increase in the line width by 45% or from 37 to 54 meV (Fig. 9(b)).

IV. DISCUSSION

The difference between the 75 meV Raman peak and the calculated harmonic E_{2g} phonon frequency (65 meV) has been attributed to the presence of anharmonic effects which are supposed to be large[8] along the entire ΓA direction. Here, we have determined using high resolution IXS the phonon dispersion and the phonon linewidth along three high symmetry directions in the Brillouin zone to verify whether anharmonic effects are relevant or not. As already shown in Refs.[25,26], the IXS phonon dispersion is in good agreement with the calculated harmonic phonon dispersion. To further determine the magnitude of anharmonic effects, in the present work, we have also measured the phonon frequency shift and linewidth as a function of temperature using Raman spectroscopy and inelastic X-ray scattering.

Our Raman spectra show a well defined peak at ≈

	$\xi = 0.0$		$\xi = 0.3$		$\xi = 0.5$		
	Raman	Theory (Anharm.)	IXS	Theory (EPC)	IXS	Theory (EPC)	Theory (Anharm.)
T=300K	53 ± 3	1.21	23 ± 2	23.0	26 ± 2	20.35	2.13
T=50K	39 ± 2	0.16	20 ± 2	23.0	24 ± 2	20.35	0.10

TABLE II: Measured (Raman and IXS) and calculated phonon-linewidth (FWHM) of the E_{2g} phonon mode at the $(0, 0, \xi)$ wave-vector in meV. Both the electron-phonon coupling (EPC) and the anharmonic contributions (Anharm.) to the phonon linewidth are reported. Computational details are explained in Refs.[23,25]. Note that the anharmonic contribution has been calculated only at selected high symmetry point: Γ ($\xi = 0.0$) and A ($\xi = 0.5$). There is no EPC contribution at Γ[28].

75 meV having E_{2g} symmetry. The energy of the 75 meV peak shifts downward and broadens by increasing the temperature. The frequency shift is more pronounced than reported by Quilty *et al.*[10] and disagrees with the finding by Martinho *et al.*[14], who reported a constant peak frequency between 10 and 300 K. The decrease in energy of the Raman-peak on temperature increase is not consistent with the claim that anharmonic four-phonon scattering is the dominant anharmonic contribution[6,8,9,12,18,19]. Indeed, since the four-phonon scattering term is positive at Γ[6,8,9,12,18,19,23], the corresponding anharmonic shift should increase with temperature (see *e.g* Eq. 4 in Ref.[23]). However, even including a negative third order term, state-of-the-art calculations[23] report a substantially smaller decrease of the E_{2g} phonon frequency than what is presently measured. *This suggests that anharmonicity is not the main mechanism determining the temperature behavior of the Raman-peak energy and that the Raman-peak is not due to a bare phonon-vibration.* We also remark that the variation of the Raman shift with the temperature (Fig. 8) cannot be explained by a two-phonon contribution as proposed by Ref.45 (see *e.g.* Ref. 35).

The large increase of the Raman linewidth between 40 K and 300 K has no equivalent in the IXS spectra. Using high-resolution IXS we have shown that the phonon linewidth along the ΓA direction is essentially temperature-independent in the 46-300 K range. This was already claimed in a previous paper[26]. However in Ref.[26] the E_{2g} peak was only detected as a shoulder of the nearby E_{1u} mode, while in the present work we have a very well resolved peak for the E_{2g} mode in the region from 0.5ΓA to A. As shown in Table II and Fig. 4 (top panel), *ab-initio* simulations are successful in predicting the phonon linewidth (including electron-phonon and anharmonic damping) of MgB_2 along all the high-symmetry directions considered. This very good agreement confirms that, in the region from 0.5ΓA to A, phonon-damping is almost exclusively due to electron-phonon coupling and not to anharmonic effects[23,25].

We finally want to stress that there is no contradiction between the Raman-peak at 75 meV *at* Γ and the X-ray E_{2g} phonon frequency at 65 meV *near* Γ and *ab-initio* harmonic calculations (giving 65 meV for the E_{2g}, Γ phonon). The key to understand these differences is the presence of relevant dynamical and electronic effects in the phonon self-energy, as shown in Ref.[24,28,29,46]. So far, ab-initio phonon calculations in MgB_2 have been performed within the adiabatic approximation. The adiabatic approximation assumes that the phonon is a *static* perturbation, but, actually, a phonon is *dynamic* perturbation, oscillating at the frequency ω. Within the adiabatic approximation, the phonon self-energy does not depend on ω, while, in general, the phonon self-energy *depends* on ω. The adiabatic approximation is valid if the interatomic force constants are istantaneous, that is the force on a given atom at a given time depends on the position of the other atoms at the same time[47]. In reality, however, the force on a given atom at a give time t depends on the position of the other atoms at a previous time t'[47]. This dynamical effect can be treated within time-dependent perturbation theory and can be relevant for zone-center optical phonons.

As shown in Refs.[24,28], the E_{2g} phonon frequency varies strongly for $\mathbf{q}$ near Γ due to dynamical effects in the real-part of the phonon self-energy. As an example, along the ΓM direction, the E_{2g} phonon frequency has a smooth behavior for $\mathbf{q} > 0.1$ΓM and increases abruptly for $\mathbf{q} < 0.05$ΓM (see fig. 3 in Refs.[24] or fig. 3(a) of Ref.[28]). The E_{2g} X-ray dynamical structure factor is strong enough for accurate statistics only for $q > 0.1$ΓM, that is IXS are probing the smooth region. On the contrary, Raman spectroscopy probes excitations at much smaller $\mathbf{q}$ ($\mathbf{q} < 0.05$ΓM), i.e. in the region where the phonon frequency is higher. Concluding, the ≈ 10 meV difference between the Raman and X-ray peaks is expected from the theoretical findings of Refs.[24,28] and is due to the pathological behavior of the phonon self-energy at Γ.

The disagreement between Raman data and the harmonic *ab-initio* calculations, published so far, is due to the fact that these calculations have been performed within the adiabatic approximation. When dynamical effects are neglected, the mentioned pathological behavior is absent[24,46] and the phonon dispersion is smooth also in the region near Γ. Therefore, the calculated E_{2g} frequency at Γ is smaller than the actual frequency, which should be computed including dynamical effects. These dynamical effects have no influence outside a small region around Γ and, for this reason, the *ab-initio* harmonic calculations done outside this region are correct and reproduce the phonon dispersion.

Finally, in Ref.[28] it was shown that the Allen formula[43] gives a zero linewidth for the E_{2g} mode at Γ. As shown in fig.5 this is not the case. To explain the presence of a non-zero linewidth at Γ, it is necessary to include electron self-energy effects in the phonon self-energy as pointed out by Cappelluti in Ref.[29]. According to Ref.[29] these effects are responsible for the unexplained softening of the Raman-peak energy and increase of the Raman-peak linewidth by increasing the temperature. However, the model of Ref.[29] is simplified, therefore giving only a qualitative trend. More theoretical work is required to achieve quantitative agreement with experiments.

V. CONCLUSIONS

We have presented a high-resolution inelastic X-ray scattering and Raman study, in order to settle the debate on the presence or not of important anharmonic effects in MgB_2. First, we have shown with high statistics and high q resolution measurements that the E_{2g} mode linewidth is independent of temperature along ΓA, ruling out a major contribution of anharmonicity in the lattice dynamics of MgB_2. Moreover we measured the dispersion along Γ-M with the best resolution to date. The E_{2g} mode shows, along this line, large variation of both phonon frequencies and line-width, as previously observed along A-L[25] and Γ-M[26] directions. Second, we have investigated the behavior of the Raman-peak energy and linewidth as a function of temperature. The Raman-peak energy decreases as a function of increasing temperature. This behavior is not reproduced by anharmonic ab-initio calculations of the E_{2g} Γ mode (calculations done both with the over-simplified frozen-phonon approach[6,8,9,12,18,19,23] or with state-of-the-art perturbation theory[23]). This finding suggests that anharmonicity is not the main mechanism determining the temperature behavior of the Raman-peak energy and that the Raman-peak is not due to a bare phonon-vibration. Finally, we have shown that, on the basis of recent theoretical results[24,28,29], there is no contradiction between the presence of a 75 meV Raman-peak at Γ and the X-ray E_{2g} phonon frequency at 65 meV *near* Γ.

In conclusion, the present results indicate that anharmonicity plays a marginal role in MgB_2. As a consequence, the explanation of the reduced isotope effect[6,7] - one of the most important unresolved issues in the physics of MgB_2 - needs to be reconsidered. At present, the explanation of the reduced isotope effect is one of the most important unresolved issues in the physics of MgB_2.

Acknowledgments

We wish to acknowledge the ESRF for the support of experiment HS-2598. The Raman measurements were performed at the Technische Universität Berlin. We thank C. Thomsen for kind hospitality in his lab, the use of the Raman equipment, and helpful discussions. We are grateful to S. Bahrs and D. Heinrich for help with the temperature-dependent Raman measurements. We thank A. Ferrari for discussion on the Raman measurements. Calculations were performed at the IDRIS supercomputing center (project 071202). This work was supported by the Swiss National Science Foundation through NCCR MaNEP.

[1] J. Nagamatsu, N. N. end T. Muranaka, Y. Zenitani, and J. Akimitsu, Nature **410**, 63 (2001).
[2] J. G. Bednorz and K. A. Müller, Z. Phys. B **64**, 189 (1986).
[3] R. J. Cava, B. Batlogg, J. J. Krajewski, R. Farrow, L. W. Rupp, A. E. White, K. Short, and W. F. P. T. Kometani, Nature **332**, 814 (1988).
[4] D. G. Hinks, H. Claus, and J. D. Jorgensen, Nature(London) **411**, 457 (2001).
[5] S. L. Bud'ko, G. Lapertot, C. Petrovic, C. E. Cunningham, N. Anderson, and P. C. Canfield, Phys. Rev. Lett **86**, 1877 (2001).
[6] H. J. Choi, D. Roundy, H. Sun, M. C. ML, and S. Louie, Nature (London) **418**, 758 (2002).
[7] H. J. Choi, D. Roundy, H. Sun, M. L. Cohen, and S. G. Louie, Phys. Rev. B **66**, 020513(R) (2002).
[8] A. Y. Liu, I. I. Mazin, and J. Kortus, Phys. Rev. Lett. **87**, 087005 (2001).
[9] J. Kortus, I. I. Mazin, K. D. Belashchenko, V. P. Antropov, and L. L. Boyer, Phys. Rev. Lett. **86**, 4656 (2001).
[10] J. W. Quilty, S. Lee, A. Yamamoto, and S. Tajima, Phys. Rev. Lett. **88**, 087001 (2002).
[11] J. W. Quilty, S. Lee, S. Tajima, and A. Yamanaka, Phys. Rev. Lett. **90**, 207006 (2003).
[12] K. P. Bohnen, R. Heid, and B. Renker, Phys. Rev. Lett. **86**, 5771 (2001).
[13] J.Hlinka, I. Gregora, J. Pokorny, A. Plecenik, P. Kus, L. Satrapinsky, and S. Benacka, Phys. Rev. B **64**, 140503(R) (2001).
[14] H. Martinho, C. Rettori, P. G. Pagliuso, A. A. Martin, N. O. Moreno, and J. L. Sarrao, Solid State Comm. **125**, 499 (2003).
[15] K. Kunc, I. Loa, K. Syassen, R. K. Kremer, and K. Ahn, J. Phys. Cond. Matt. **13**, 9945 (2001).
[16] P. M. Rafailov, M. Dworzak, and C. Thomsen, Solid State Comm. **122**, 455 (2002).
[17] D. DiCastro, E. Cappelluti, M. Lavagnini, A. Sacchetti, A. Palenzona, M. Putti, and P. Postorino, Phys. Rev. B **74**, 100505(R) (2006).
[18] T. Yildirim, O. Gülseren, J. W. Lynn, C. M. Brown, T. J. Udovic, Q. Huang, N. Rogado, K. A. Regan, M. A. Hayward, J. S. Slusky, et al., Phys. Rev. Lett. **87**, 037001 (2001).
[19] L. Boeri, G. B. Bachelet, E. Cappelluti, and L. Pietronero, Phys. Rev. B **65**, 214501 (2002).
[20] J. Menéndez and M. Cardona, Phys. Rev. B **29**, 2051 (1984).

[21] A. Debernardi, S. Baroni, and E. Molinari, Phys. Rev. Lett. **75**, 1819 (1995).

[22] G. Lang, K. Karch, M. Schmitt, P. Pavone, A. P. Mayer, R. K. Wehner, and D. Strauch, Phys. Rev. B **59**, 6182 (1999).

[23] M. Lazzeri, M. Calandra, and F. Mauri, Phys. Rev. B **68**, 220509(R) (2003).

[24] M. Calandra, M. Lazzeri, and F. Mauri, accepted Physica C (2007).

[25] A. Shukla, M. Calandra, M. d'Astuto, M. Lazzeri, F. Mauri, C. Bellin, M. Krisch, J. Karpinski, S. M. Kazakov, J. Jun, et al., Phys. Rev. Lett. **90**, 095506 (2003).

[26] A. Q. R. Baron, H. Uchiyama, Y. Tanaka, S. Tsutsui, D. Ishikawa, S. Lee, R. Heid, K.-P. Bohnen, S. Tajima, and T. Ishikawa, Phys. Rev. Lett. **92**, 197004 (2004).

[27] Y. Kong, O. V. Dolgov, O. Jepsen, and O. K. Andersen, Phys. Rev. B **64**, 020501(R) (2001).

[28] M. Calandra and F. Mauri, Phys. Rev. B **71**, 064501 (2005).

[29] E. Cappelluti, Phys. Rev. B **73**, 140505(R) (2006).

[30] R. Verbeni, F. Sette, M. Krisch, U. Bergmann, B. Gorges, C. Halcoussis, K. Martel, C. Masciovecchio, J. Ribois, G. Ruocco, et al., J. Synchrotron Radiation **3**, 62 (1996).

[31] C. Masciovecchio, U. Bergmann, M. Krisch, G. Ruocco, F. Sette, and R. Verbeni, Nucl. Instrum. Meth. B **111**, 181 (1996).

[32] C. Masciovecchio, U. Bergmann, M. Krisch, G. Ruocco, F. Sette, and R. Verbeni, Nucl. Instrum. Meth. B **117**, 339 (1996).

[33] A. Bergamin, G. Cavagnero, and G. Mana, J. Appl. Phys. **82**, 5396 (1997).

[34] F. James, *MINUIT Function Minimization and Error Analysis*, Computing and Networks Division, CERN, Geneva (1998), (CERN D506 Long Writeup).

[35] M. Cardona, in *Light Scattering in Solids II*, edited by M. Cardona and G. Güntherodt (Springer, Berlin, 1982), vol. 50 of *Topics in Applied Physics*, chap. 2, p. 19.

[36] X. K. Chen, M. J. Konstantinovic, J. C. Irwin, D. D. Lawrie, and J. P. Franck, Phys. Rev. Lett. **87**, 157002 (2001).

[37] S. Baroni, S. de Gironcoli, A. D. Corso, and P. Giannozzi, Rev. Mod. Phys **73**, 515 (2001).

[38] Baroni *et al.*, PWSCF/espresso code is available at http://www.pwscf.org.

[39] J.P.Perdew, K.Burke, and M.Ernzerhof, Phys. Rev. Lett. **77**, 3865 (1996).

[40] N. Troullier and J. L. Martins, Phys. Rev. B **43**, 1993 (1991).

[41] S. G. Louie, S. Froyen, and M. L. Cohen, Phys. Rev. B **26**, 1738 (1982).

[42] S. de Gironcoli, Phys. Rev. B **51**, 6773 (1995).

[43] P. B. Allen, Phys. Rev. B **6**, 2577 (1972), P. B. Allen and R. Silberglitt, Phys. Rev. B **9**, 4733 (1974).

[44] D. Waasmaier and A. Kirfel, Acta Cryst. **A51**, 416 (1995).

[45] A. Q. R. Baron, H. Uchiyama, R. Heid, K. P. Bohnen, Y. Tanaka, S. Tsutsui, D. Ishikawa, S. Lee, and S. Tajima, Phys. Rev. B **75**, 020505(R) (2007).

[46] M. Lazzeri and F. Mauri, Phys. Rev. Lett. **97**, 266407 (2006).

[47] P. Allen, in *Metals, superconductors, magnetic materials, liquids*, edited by G. Horton and A. Maradudin (North-Holland Publishing Company, Amsterdam, New York, 1980), vol. 3 of *Dynamical Proiperties of Solids*, chap. 2, p. 95.